TURBULENT BOUNDARY LAYER INDUCED NOISE AND VIBRATION OF A MULTI-PANEL WALLED ACOUSTIC ENCLOSURE

Joana da Rocha[1], Afzal Suleman[1], and Fernando Lau[2]
[1]Dept. of Mechanical Engineering, University of Victoria, PO Box 3055, Stn. CSC, Victoria, BC, Canada, V8W 3P6
jdarocha@uvic.ca, suleman@uvic.ca
[2]Centro de Ciências e Tecnologias Aeronáuticas, Dept. de Engenharia Mecânica, Instituto Superior Técnico, Av. Rovisco Pais, Lisboa, Portugal, 1049-001 lau@ist.utl.pt

ABSTRACT

Flow-induced noise in aircraft cabins can be predicted through analytical models or numerical methods. To date, analytical methods have been used for simple structures and cabins, where usually a single panel is vibrating due to the flow excitation, and coupled with an acoustic enclosure. The present work investigates the analytical prediction of turbulent boundary layer induced noise and vibration of a multi-panel system. The objective is to investigate the coupling between individual panels and the acoustic enclosure. Each panel is coupled with the acoustic enclosure, which consists of a large rectangular room, with five rigid walls and one flexible wall. The properties of the panels and acoustic enclosure represent a typical fuselage skin panel and a cabin section, respectively. It is shown that identical panels located at different positions have dissimilar contributions to the cabin interior noise, showing that the panel position is an important variable for the accurate prediction and suppression of cabin noise. Analytical predictions were obtained for both the space-averaged interior sound pressure level and local interior sound pressure level. The space-averaged sound pressure level is usually accepted to provide the necessary information for the noise prediction; however, in some real life applications, the local sound pressure may also be desirable.

RÉSUMÉ

Le bruit à l'intérieur d'es cabines d´es avions induite par écoulement externe peut être prédit par modèles analytiques ou méthodes numériques. À ce jour, les méthodes analytiques ont été utilisés pour structures et chambre simples, où, normalement, un seul panneau est considéré à vibrer en raison de l'écoulement externe, et couplé avec la chambre acoustique. Cet article étudie la prévision analytique des vibrations et du bruit dans un système avec plusieurs panneaux. L'objectif est d´examiner le couplage entre panneaux individuels et la chambre acoustique, en considérant de l'emplacement du panneau comme une variable. La cabine acoustique est une grande chambre rectangulaire et les panneaux rectangulaires sont considérés simplement appuyés. Les propriétés des matériaux et les dimensions des panneaux et de chambre acoustique sont représentatives d'un panneau de fuselage typique d'un avion et un compartiment de la cabine, respectivement. Il est conclu que panneaux similaires situés dans des positions différentes de la cabine ont contributions différentes du bruit intérieur, montrant que la position du panneau est une variable importante pour une prévision précise de bruit et de suppression de bruit dans la cabine. Ont été obtenu des prévisions analytiques des valeurs localisées du niveau de pression sonore à l'intérieur, et la moyenne de ces valeurs en l'espace. Le niveau moyen de pression acoustique à l'intérieur est habituellement utilisé pour obtenir information de la prévision du bruit; cependant, dans certaines situations et applications réelles, la valeur du niveau de pression acoustique d'un point précis dans l'espace peut être souhaitable.

1. INTRODUCTION

The turbulent boundary layer (TBL) induced vibration in transport vehicles, particularly in aircraft, is a major source of interior noise, and thus an important topic of investigation. As confirmed by flight measurements in [1], the interior noise in the cabin of a jet transport aircraft, during cruise flight, is mostly generated by the external TBL excitation. While during takeoff the engine noise is the dominant source of cabin noise, the airflow sources become the major contribution for the interior noise during cruise flight. For subsonic flight, the TBL pressure levels on the exterior of the fuselage increase with the flight speed [2–4], representing a major source of aircraft interior noise for frequencies below 1000 Hz [1, 5]. Specifically, in [6], flight test measurements in an aircraft cockpit indicated that interior noise was dominated by low-frequency noise (<500 Hz), and that the main noise source was the external turbulent flow. As referred in [7], TBL excitation is regarded as the most important noise source for jet powered aircraft at cruise speed, particularly, as new quieter jet engines are being developed.

The main objective of the present work is the development of accurate analytical models for the prediction of TBL-induced noise in the interior of a real scale rectangular cabin. The physical system considered corresponds to a rectangular shaped acoustic enclosure, filled with air, with one flexible wall and five rigid walls. The flexible wall is composed of 50 identical simply supported panels. The dimensions and properties of the plates are similar to those of typical aircraft fuselage skin panels. A larger acoustic enclosure, compared with the plate's dimensions, was studied in order to simulate a more realistic approach of an aircraft fuselage section. Both the unpressurized and pressurized cabin are explored. The external flow excitation is representative of typical cruise conditions of a commercial aircraft, i.e., of the TBL wall pressure fluctuations in the aircraft fuselage, while in cruise and stabilized flight conditions. The TBL is assumed to be attached and completely developed over the aircraft structure. The amplitude of the wall pressure fluctuations is dependent on the TBL thickness, thus depends on the longitudinal position of the plate.

Previous work performed by the authors has validated the analytical models for single panel coupled with an acoustic enclosure, as in [8]. The analytical framework was successfully validated through comparison with several independent experimental studies. The present work adds a step forward compared to previous studies - it considers the TBL as the panel's excitation, while considering each panel (located at different positions in the flexible wall) coupled with a real scaled acoustic enclosure. The aim is to investigate the coupling between individual panels and the acoustic enclosure. It is shown that the position of the plate relative to the enclosure plays a crucial role in the accurate prediction of the interior pressure field. The difference between predicted space-averaged sound pressure level (SASPL) and predicted local sound pressure level (LSPL) is also explored.

The analytical formulation was developed from the fundamental equations and intrinsically derived as a structural-acoustic coupled model, i.e., it accounts for the natural modes of the plate and the acoustic modes of the enclosure. A convergence study was performed to calculate the minimum number of plate and acoustic modes needed for convergence of the predicted spectral quantities. Results were obtained for the prediction of vibration and sound pressure levels in the power spectral density (PSD) domain, up to a frequency of 1000 Hz. The model is able to predict the space-average plate displacement level, the space-average interior SPL, local plate displacement level (at a specified location on the panel surface), and local SPL. The occurrence of the hydrodynamic coincidence phenomenon is also investigated.

1.1 Turbulent Boundary Layer Excited Panels

Previous investigations on flow-induced noise and vibration have been reported, although, it is important to recognize how different these studies are, and how their nature can affect the development of a predictive mathematical model. Specifically, the study of the noise radiation by a isolated panel into free air, involves a different analysis compared with the study of cabin interior noise prediction due to the vibration of a panel. The later involves the coupling between the structural vibration and the cabin acoustic field. When the purpose is to develop analytical models for the prediction of cabin noise levels, one needs to consider the properties of: (1) the excitation, (2) the vibrating structure, and (3) the sound receiving room.

Several early experimental studies were performed to investigate the vibration and radiation of sound from structural panels, excited by the TBL, e.g. [9–12]. These studies provide knowledge about the shape of the spectrum, convection velocity and space-time correlation of the exterior TBL pressure fluctuations on aircraft panels, as well as displacement and acceleration spectra of the vibrating aircraft panels. Additionally, theoretical studies have also been performed to study the vibration and sound radiated by isolated panels (i.e., not coupled with an acoustic enclosure) excited by turbulent flows [13–17], and for random vibration of a single panel coupled with a small acoustic enclosure [7, 18, 19]. In these studies, the TBL excitation is usually described in terms of the statistical properties of the wall pressure fluctuations based on the Corcos formulation [20, 21]. Even though a number of new models were developed after the Corcos model for the TBL description, e.g. [22–25], the Corcos formulation is widely used in recent studies to describe the TBL pressure field [26–30], since it captures the fundamental pressure tendency along the frequency and requires significantly reduced computational effort to employ. Furthermore, Corcos formulation provides a good estimation for the TBL wall-pressure fluctuations levels at and near the convective peak, which is of fundamental importance for aircraft boundary layers (for high subsonic Mach numbers) [26], the case of the present study. In order to account with the streamwize variation of the boundary layer thickness, in the present study the Efimtsov model [22] is used to provide the point power spectrum. In the comparison of the several models available to describe the turbulent boundary layer wall pressure in [31], the model developed by Efimtsov is cited as a suitable candidate, being the only model derived from aircraft flight tests rather than laboratory measurements. More recently, flight tests performed in the Tupolev 144LL aircraft [32], demonstrated that the Efimtsov model shows the best agreement with the experimental data.

In the present study, the panels are considered to be simply supported in all four edges. Each panel represents the distance between adjacent stringers and frames (no additional stiffeners are considered), and is individually vibrating and coupled with the acoustic enclosure. As concluded in [11, 33], while jet noise induced vibration is highly correlated over several panels in both longitudinal and circumferential directions, the TBL induced vibration (in which the vibration correlation decays rapidly especially

in the circumferential direction) is confined to one or two adjacent panels in the longitudinal direction. For the TBL excitation, the vibration of an isolated panel can be considered with the limitation that it is not necessarily valid at frequencies below the lowest natural frequency of a single bay of the fuselage structure (which in the present study is 61.44 Hz for the unpressurized cabin, and 355.45 Hz for the pressurized cabin).

1.2 Aircraft Cabin Noise Induced by Turbulent Flow

Several experimental studies were conducted to investigate the aircraft cabin interior noise induced by the TBL [34–37], providing measurements of the interior SPL and fuselage skin vibrations spectrum, at various locations in the cabin and cockpit of commercial aircraft, for aluminum and composite fuselages. These studies are a good database for comparison with theoretical predictions of interior noise levels induced by the TBL. The effect of aircraft speed on boundary layer induced interior noise can be seen to be dramatic, with the interior sound pressure levels being generally higher for higher flight speeds. The TBL wall pressure levels increase with the flight Mach number, as concluded in [2, 4, 33]. In the absence of hydrodynamic coincidence phenomenon, the interior noise level usually follows the same tendency, i.e., it increases with the flight Mach number [7, 16, 38]. In the presence of hydrodynamic coincidence, the tendency of increased interior noise with higher flight speeds is generally valid for frequencies below and above the neighborhood of frequency at which hydrodynamic coincidence occurs, as shown in [11].

Interior cabin noise is a challenging problem in most aircraft and many other transport vehicles. The reduction of cabin noise levels is desirable for both comfort and health-related reasons, and they are balanced with the cost, complexity, and physical constraints of noise control systems. As well known, passive noise control techniques are not effective in the low-frequency noise range, where the active noise control techniques have demonstrated better results, showing the ability to decrease sound levels without a big penalty in terms of weight. However, because of the complexity of the coupled structural-acoustic system, the implementation of these techniques is far from being straightforward. To efficiently design a noise control system, a clear understanding of the mechanisms of sound radiation and transmission of the coupled structural-acoustic system is crucial. In this context, the objective of the present study is to contribute for the understanding of the sound transmission phenomenon involved in the multi-panel structural-acoustic system.

2. MATHEMATICAL MODELS

In this section, the mathematical models developed are presented. Three models need to be defined: (1) the TBL model, which represents the external force applied to each panel, (2) the structural model, representing each individual plate coupled with the acoustic enclosure, and (3) the acoustic model, consisting of a rectangular acoustic cabin. In the following subsections, the mathematical models involved in the analysis are presented. Since previous work was performed in order to validate the analytical model, for simple systems, in this work the new developments on the model are emphasized. If the reader wishes to see more details of the mathematical manipulations involved in the analysis, please refer to [8].

2.1 Turbulent Flow Model

As previously referred, modeling the TBL wall pressure has been a subject of study for many years. Since the TBL is a random process, the resultant wall pressure, p(x, y, t), is usually statistically described in terms of the pressure power spectral density (PSD). These models were developed for turbulent flow over a flat plate, assuming fully developed flow and zero mean pressure gradient. For these conditions, the turbulent flow can be regarded as stationary in time and homogeneous in space. The cross-spectral density of the wall pressure over the (x, y) plane, for flow in the x-direction, can be defined through the Corcos formulation [20, 21], as follows

$$S(x,\xi_x,\xi_y,\omega) = S_{ref}(x,\omega)\, e^{-\frac{\alpha_x \omega |\xi_x|}{U_c}}\, e^{-\frac{\alpha_y \omega |\xi_y|}{U_c}}\, e^{-\frac{i\omega\xi_x}{U_c}}, \quad (1)$$

in which ξ_x and ξ_y are the spatial separations in the streamwise and spanwise directions of the plate, respectively, ω is the angular frequency, U_c is the convective speed of the TBL, and α_x and α_y are empirical parameters that denote the lost of coherence in the longitudinal and transverse directions, and are chosen to yield the best agreement with the reality. Recommended empirical values for aircraft boundary layers are $\alpha_x = 0.1$ and $\alpha_y = 0.77$ [31]. Note that, with relation to previous study [8], x was added as a variable for the $S(x,\xi_x,\xi_y,\omega)$ and $S_{ref}(x,\omega)$ terms. This variable needs to be added since the TBL pressure cross-spectral density dependents on the position of each panel; i.e., panels positioned at different x-coordinates have different S_{ref} values. Efimtsov model, defined in [22], is in good agreement with experimental data for the flow speed of interest in the present work, and provide the reference PSD as follows:

$$S_{ref}(x,\omega) = \frac{\tau_w^2(x)\,\delta(x)}{U_\tau(x)}\,\frac{0.01\,\pi}{1+0.02\,Sh^{2/3}(x,\omega)}, \quad (2)$$

with:

$$U_\tau(x) = U_\infty\sqrt{\frac{C_f(x)}{2}},\ \tau_w(x) = \frac{1}{2}\rho U_\infty^2 C_f(x),\ Sh(x,\omega) = \frac{\omega\,\delta(x)}{U_\tau(x)}, \quad (3)$$

where U_τ is the friction velocity, τ_w is the mean wall shear stress, C_f is the friction coefficient, δ is the boundary layer thickness, Sh is the Strouhal number, and U_∞ is the free-stream velocity. Functions $C_f(x)$ and $\delta(x)$ were computed using the following semi-empirical expressions for turbulent

boundary layers, respectively from [39] and [9]:

$$C_f(x) = 0.37(\mathrm{Log}_{10}\mathrm{Re}_x)^{-2.584}, \quad (4a)$$

$$\delta(x) = 0.37\ x\ \mathrm{Re}_x^{-\frac{1}{5}}\left[1+\left(\frac{\mathrm{Re}_x}{6.9\times10^7}\right)^2\right]^{\frac{1}{10}}. \quad (4b)$$

Values of C_f and δ for each plate are shown in Fig. 1. Plates located at the same x-coordinate have same values of C_f and δ. In these figures, points x_1 through x_5 correspond to the panel center locations from the first to the fifth rows of panels along x-direction. Points x_i and x_f correspond, respectively, to the x-coordinate in which the first row of panels starts (i.e., to x = 9.14 m) and to the x coordinate in which the last row of panels ends (i.e., x = 11.64 m) - refer to Fig. 3 for more details about the physical system under study. Fig. 2 shows $S_{ref}(x,\omega)$ for different flight speeds and altitudes, given by Eq.(2), for the fifth row of panels. For this row of panels, the curve corresponding to the present study is the one with solid line and bold circle – refer to Table 2 for more information about external fluid parameters. As concluded in [32], the predictions provided by the Efimtsov model, using Eq.(2), show a weaker decay than the measured data at high frequencies (above 1000 Hz), over predicting the spectral quantities above this frequency. Since the present study considers only frequencies up to 1 KHz, this problem does not significantly affect the results.

2.2 Panels Displacement Model

All plates are considered to be flat panels, simply supported in all four boundaries (as in Fig. 3b) and are assumed to represent the distance between adjacent stringers and frames of a conventional aircraft skin-stringer-frame structure. The displacement of each panel is defined in terms of its natural modes, as follows

$$w(x,y,t) = \sum_{m_x=1}^{M_x}\sum_{m_y=1}^{M_y} \alpha_{m_x}(x)\,\beta_{m_y}(y)\,q_{m_x m_y}(t), \quad (5)$$

where $\alpha_{m_x}(x)$ and $\beta_{m_y}(y)$ functions define the variation of w with the x and y, respectively, $q_{m_x m_y}(t)$ define the variation of w with t, and $M = M_x \times M_y$ is the total number of plate modes considered in the analysis. As shown in Fig. 3a, the direction of the plate displacement, w, was chosen to be the positive z-direction. Since the panels are simply supported plates, the spatial functions may be defined, in the plate (local) coordinates system, as:

$$\alpha_{m_x}(x_1) = \sqrt{\frac{2}{a}}\ \sin\left(\frac{m_x\,\pi\,x_1}{a}\right), \quad (6a)$$

$$\beta_{m_y}(y_1) = \sqrt{\frac{2}{b}}\ \sin\left(\frac{m_y\,\pi\,y_1}{b}\right), \quad (6b)$$

in which a and b are the dimensions of the plate in the x- and y-directions.

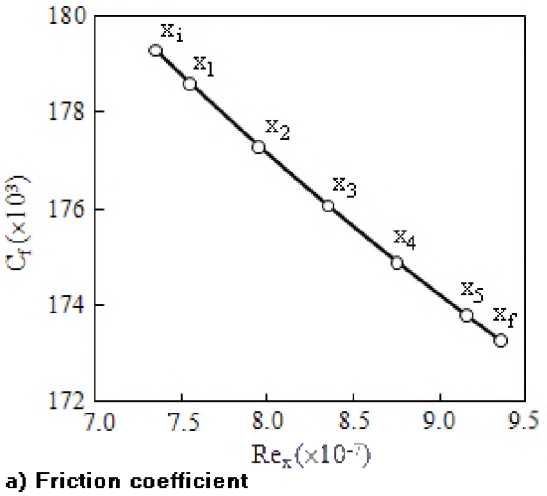

a) Friction coefficient

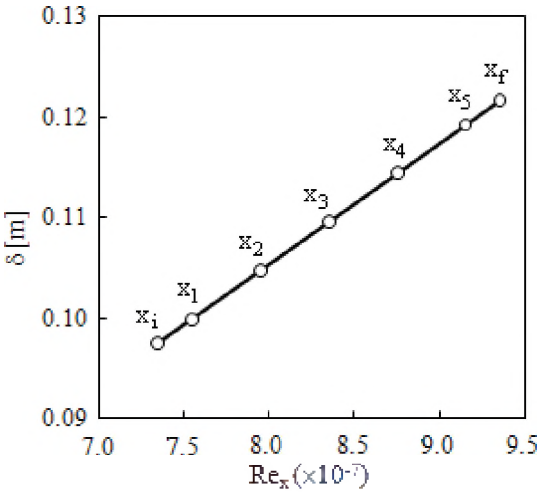

b) Boundary layer thickness

Figure 1. Comparison of the C_f and δ values along the several x panel rows.

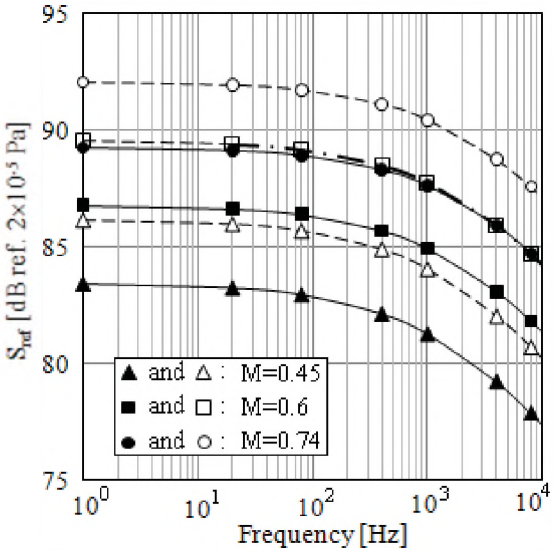

Figure 2. Reference PSD obtained from Efimtsov model, for altitudes 25000 ft (solid lines) and 16400 ft (dashed lines).

However, in order to compute the structural-acoustic coupling, it is convenient to work in the enclosure (global) coordinates system. To accomplish that, Eqs.(6) can be written in the global coordinates system, for each individual plate, as follows:

$$\alpha_{m_x}(x) = \sqrt{\frac{2}{a}} \sin\left(\frac{m_x \pi (x-x_{p_i})}{a}\right), \quad (7a)$$

$$\beta_{m_y}(y) = \sqrt{\frac{2}{b}} \sin\left(\frac{m_y \pi (y-y_{p_i})}{b}\right), \quad (7b)$$

where (x_{pi}, y_{pi}) is the position of the origin of the i^{th} plate coordinates system, written in the global coordinates system. The natural frequencies for the simply supported untensioned plate (unpressurized cabin) and tensioned plate (pressurized cabin), are given respectively by:

$$\omega^p_{m_x m_y} = \sqrt{\frac{D_p}{\rho_p h_p}} \left[\left(\frac{m_x \pi}{a}\right)^2 + \left(\frac{m_y \pi}{b}\right)^2\right], \quad (8a)$$

$$\omega^p_{m_x m_y} = \sqrt{\frac{1}{\rho_p h_p}\left[D_p(f_x{}^2 + g_y{}^2)^2 + T_x f_x{}^2 + T_y g_y{}^2\right]}, \quad (8b)$$

in which ρ_p is the density of the panel, h_p is its thickness, $D_p = \frac{E_p h_p^3}{12(1-\nu_p^2)}$ is the panel stiffness constant, T_x and T_y are the in-plane tensions in x- and y-directions, respectively, and $f_x = \frac{m_x \pi}{a}$ and $g_y = \frac{m_y \pi}{b}$. The plate governing equations for a given applied external pressure, for the unpressurized and pressurized cabins, are respectively:

$$D_p \nabla^4 w + \rho_p h_p \ddot{w} + \zeta_p \dot{w} = p_{ext}(x,y,t), \quad (9a)$$

$$D_p \nabla^4 w + \rho_p h_p \ddot{w} + \zeta_p \dot{w} - (T_x f_x{}^2 + T_y g_y{}^2) w = p_{ext}(x,y,t), \quad (9b)$$

where ζ_p was added to account for the damping of the plate, and w is given by Eq.(5).

2.3 Acoustic Cabin Pressure Model

Following the same approach as for the plate's displacement models, the pressure inside the enclosure is defined in terms of the acoustic modes, as follows:

$$p(x,y,z,t) = \sum_{n_x=1}^{N_x} \sum_{n_y=1}^{N_y} \sum_{n_z=1}^{N_z} \psi_{n_x}(x)\, \phi_{n_y}(y)\, \Gamma_{n_z}(z)\, r_{n_x n_y n_z}(t), \quad (10)$$

where $\psi_{n_x}(x)$, $\phi_{n_y}(y)$ and $\Gamma_{n_z}(z)$ are spatial functions, $r_{n_x n_y n_z}(t)$ are functions of t, and $N = (N_x+1)\times(N_y+1)\times(N_z+1)$ is the number of acoustics modes considered. As shown in Fig. 3a, the direction of the interior pressure, p, was chosen to be the positive z-direction. The individual spatial functions are assumed to be orthogonal between each other, and given by the rigid body enclosure modes, as follows:

$$\psi_{n_x}(x) = \frac{A_{n_x}}{\sqrt{L_x}} \cos\left(\frac{n_x \pi x}{L_x}\right), \quad (11a)$$

$$\phi_{n_y}(y) = \frac{A_{n_y}}{\sqrt{L_y}} \cos\left(\frac{n_y \pi y}{L_y}\right), \quad (11b)$$

$$\Gamma_{n_z}(z) = \frac{A_{n_z}}{\sqrt{L_z}} \cos\left(\frac{n_z \pi z}{L_z}\right), \quad (11c)$$

where L_x, L_y and L_z are the dimensions of the enclosure in the x-, y- and z-directions, respectively, and the constants A_n were chosen to satisfy normalization. For a rectangular cavity, the natural frequencies are determined as follows:

$$\omega^{ac}_{n_x n_y n_z} = c_0 \sqrt{\left(\frac{n_x \pi}{L_x}\right)^2 + \left(\frac{n_y \pi}{L_y}\right)^2 + \left(\frac{n_z \pi}{L_z}\right)^2}, \quad (12)$$

where c_0 is the speed of sound inside the acoustic enclosure. The governing equation is the wave equation, defined by

$$\nabla^2 p - \frac{1}{c_0^2} \ddot{p} - \zeta_{ac} \dot{p} = 0, \quad (13)$$

in which ζ_{ac} was added to account for the acoustic damping in the enclosure.

2.4 Coupled System Model

To obtain the governing equations of the coupled structural-acoustic system, the equations of the individual uncoupled subsystems should be combined (please refer to [8] for the coupling details). The equations of the coupled plate-enclosure system can be written together in the matrix form, as follows:

$$\begin{bmatrix} \mathbf{M}_{pp} & \mathbf{0} \\ \mathbf{M}_{cp} & \mathbf{M}_{cc} \end{bmatrix} \begin{Bmatrix} \ddot{\mathbf{q}}(t) \\ \ddot{\mathbf{r}}(t) \end{Bmatrix} + \begin{bmatrix} \mathbf{D}_{pp} & \mathbf{0} \\ \mathbf{0} & \mathbf{D}_{cc} \end{bmatrix} \begin{Bmatrix} \dot{\mathbf{q}}(t) \\ \dot{\mathbf{r}}(t) \end{Bmatrix} + \begin{bmatrix} \mathbf{K}_{pp} & \mathbf{K}_{pc} \\ \mathbf{0} & \mathbf{K}_{cc} \end{bmatrix} \begin{Bmatrix} \mathbf{q}(t) \\ \mathbf{r}(t) \end{Bmatrix} = \begin{Bmatrix} \mathbf{p}_{tbl}(t) \\ \mathbf{0} \end{Bmatrix}, \quad (14)$$

with:

$$\mathbf{M}_{pp} = \mathrm{diag}\left[\rho_p h_p\right] \quad \text{and} \quad \mathbf{M}_{cc} = \mathrm{diag}\left[\frac{1}{c_0^2}\right], \quad (15a)$$

$$\mathbf{M}_{cp} = \rho_0 \left[\frac{(-1)^{n_z} A_{n_z}}{\sqrt{L_z}} \int_{x_{p_i}}^{x_{p_f}} \alpha_{m_x}(x)\psi_{n_x}(x)dx \int_{y_{p_i}}^{y_{p_f}} \beta_{m_y}(y)\phi_{n_y}(y)dy\right], \quad (15b)$$

$$\mathbf{D}_{pp} = \mathrm{diag}\left[2\rho_p h_p \omega_m \xi_p\right] \quad \text{and} \quad \mathbf{D}_{cc} = \mathrm{diag}\left[2\frac{1}{c_0^2}\omega_n \xi_{ac}\right], \quad (15c)$$

$$\mathbf{K}_{pp} = \mathrm{diag}\left[\omega_m^2\ \rho_p\ h_p\right] \quad \text{and} \quad \mathbf{K}_{cc} = \mathrm{diag}\left[\omega_n^2\ \frac{1}{c_0^2}\right], \tag{15d}$$

$$\mathbf{K}_{pc} = -\left[\frac{(-1)^{n_z} A_{n_z}}{\sqrt{L_z}} \int_{x_{p_i}}^{x_{p_f}} \alpha_{m_x}(x)\psi_{n_x}(x)dx \int_{y_{p_i}}^{y_{p_f}} \beta_{m_y}(y)\phi_{n_y}(y)dy\right], \tag{15e}$$

$$\mathbf{p}_{tbl}(t) = -\left[\int_{y_{p_i}}^{y_{p_f}} \int_{x_{p_i}}^{x_{p_f}} \alpha_{m_x}(x)\ \beta_{m_y}(y)\ p_{tbl}(x,y,t)\ dx\ dy\right]. \tag{15f}$$

In the previous equations, **M** represents mass matrices, **D** damping matrices, **K** stiffness matrices, subscripts *p* and *c* correspond respectively to *plate* and *cavity*. All matrices and vectors expressions were obtained analytically as shown in [8]. Additionally, $\zeta_p = 2\omega_m\xi_p$ is the structural modal damping and $\zeta_{ac} = 2\omega_n\xi_{ac}$ is the acoustic modal damping. For notation simplicity, $\omega^p_{m_x m_y}$, $\omega^{ac}_{n_x n_y n_z}$, $q_{m_x m_y}(t)$, and $r_{n_x n_y n_z}(t)$ were substituted, respectively, by ω_m , ω_n, $q_m(t)$ and $r_n(t)$. Note that ω_m, in Eqs.(15), is given by Eq.(8a) for the unpressurized cabin and by Eq.(8b) for the pressurized cabin. The cross terms, i.e., matrices $\mathbf{M_{cp}}$ and $\mathbf{K_{pc}}$, are responsible for the coupling between each panel displacement and the enclosure pressure. Note that Eq.(14) accounts for the coupling of only one plate with the enclosure, i.e., the contribution of each panel for the interior sound pressure level is individually analyzed.

3. SOLUTION IN THE SPECTRAL DOMAIN

Since the TBL wall pressure field model is expressed in the frequency domain, one needs to transform the equation of the coupled system, Eq.(14), from the time domain to the frequency domain. As introduced in [8], this can be performed by assuming $q_m = Q_m\, e^{i\omega t}$ and $r_n = R_n\, e^{i\omega t}$. The spectral density of the system response is then given by:

$$\mathbf{S_{YY}}(\omega) = \mathbf{H}^*(\omega)\ \mathbf{S_{XX}}(\omega)\ \mathbf{H}^T(\omega)\ , \tag{16}$$

in which superscripts * and T denote, respectively, Hermitian conjugate and matrix transpose, $\mathbf{S_{XX}}(\omega)$ is the spectral density matrix of the excitation, and $\mathbf{S_{YY}}(\omega)$ is the spectral density of the system response. For mathematical convenience, matrix $\mathbf{S_{YY}}(\omega)$ can be divided in two matrices: (1) the PSD matrix of the coupled plate displacement, $\mathbf{S_{WW}}(\omega)$, and (2) the PSD matrix of the coupled acoustic enclosure pressure, $\mathbf{S_{PP}}(\omega)$. Similarly, matrix $\mathbf{S_{XX}}(\omega)$ can be divided in: (1) the PSD matrix of the turbulent boundary layer excitation, $\mathbf{S_{tbl}}(\omega)$, and (2) a null matrix. Considering this, Eq.(16) can be written in the following separate form:

$$\mathbf{S_{WW}}(\omega) = \mathbf{H_W}^*(\omega)\ \mathbf{S_{tbl}}(\omega)\ \mathbf{H_W}^T(\omega)\ , \tag{17a}$$

$$\mathbf{S_{PP}}(\omega) = \mathbf{H_P}^*(\omega)\ \mathbf{S_{tbl}}(\omega)\ \mathbf{H_P}^T(\omega)\ , \tag{17b}$$

where matrices $\mathbf{H_W}(\omega)$ and $\mathbf{H_P}(\omega)$ are defined by:

$$\mathbf{H_W}(\omega) = (\mathbf{A} - \mathbf{B}\,\mathbf{D}^{-1}\,\mathbf{C})^{-1}, \tag{18a}$$

$$\mathbf{H_P}(\omega) = -\,\mathbf{D}^{-1}\,\mathbf{C}\,\mathbf{H_W}(\omega)\ , \tag{18b}$$

and

$$\mathbf{A} = -\,\omega^2\,\mathbf{M_{pp}} + i\,\omega\,\mathbf{D_{pp}} + \mathbf{K_{pp}}\,, \tag{19a}$$

$$\mathbf{B} = \mathbf{K_{pc}}\ , \tag{19b}$$

$$\mathbf{C} = -\,\omega^2\,\mathbf{M_{cp}}\ , \tag{19c}$$

$$\mathbf{D} = -\,\omega^2\,\mathbf{M_{cc}} + i\,\omega\,\mathbf{D_{cc}} + \mathbf{K_{cc}}\ . \tag{19d}$$

The generalized PSD matrix of the TBL excitation, $\mathbf{S_{tbl}}(\omega)$, the PSD function of the plate´s displacement, and the PSD function of the enclosure interior pressure are defined, respectively, as follows:

$$\mathbf{S_{tbl}}(\omega) = \left[\int_{S_p}\int_{S_p} \alpha_{m_x}(x)\alpha_{m_{x'}}(x')\beta_{m_y}(y)\beta_{m_{y'}}(y')S(x,\xi_x,\xi_y,\omega)dSdS'\right], \tag{20}$$

$$S_{ww}(x_1, y_1, x_2, y_2, \omega) = \sum_{m_{x_1}, m_{x_2}=1}^{M_x^2} \sum_{m_{y_1}, m_{y_2}=1}^{M_y^2} \alpha_{m_{x_1}}(x_1)\alpha_{m_{x_2}}(x_2)\beta_{m_{y_1}}(y_1)\beta_{m_{y_2}}(y_2)\mathbf{S_{WW}}(\omega)_{m_1,m_2} \tag{21}$$

$$S_{pp}(x_1, y_1, z_1, x_2, y_2, z_2, \omega) = \sum_{n_{x_1}, n_{x_2}=1}^{N_x^2} \sum_{n_{y_1}, n_{y_2}=1}^{N_y^2} \sum_{n_{z_1}, n_{z_2}=1}^{N_z^2} \psi_{n_{x_1}}(x_1)\psi_{n_{x_2}}(x_2)\phi_{n_{y_1}}(y_1)\phi_{n_{y_2}}(y_2)\Gamma_{n_{z_1}}(z_1)\Gamma_{n_{z_2}}(z_2)\ \mathbf{S_{PP}}(\omega)_{n_1,n_2} \tag{22}$$

in which $S_p = a \times b$ is the plate surface area. Eqs.(21) and (22) can be used to predict the displacement PSD at a chosen point in the plate, and the pressure PSD at any given location of the acoustic enclosure, respectively. Finally, the space-averaged PSD functions can be found by integrating the individual power spectral densities over the plate area and the cavity volume, respectively, as:

$$S_{ww}(\omega) = \int_{S_p}\int_{S_p} S_{ww}(x_1, y_1, x_2, y_2, \omega)\ dS_1 dS_2, \tag{23}$$

$$S_{pp}(\omega) = \int_{V_e}\int_{V_e} S_{pp}(x_1,y_1,z_1,x_2,y_2,z_2,\omega)\ dV_1 dV_2, \tag{24}$$

in which $V_c = L_x \times L_y \times L_z$ is the enclosure volume. The analytical expressions derived for $S_{tbl}(\omega)$, $S_{ww}(\omega)$ and $S_{pp}(\omega)$ are shown [8].

4. PHYSICAL SYSTEM

The geometry of the complete system is shown in Fig. 3. The turbulent flow is developed across the plates, at $z = L_z$, in the positive x-direction. The dimensions of the system are given in Table 1 and the physical parameters, including the external fluid, the plate, and the acoustic enclosure are listed in Table 2. The properties of the plates are for aluminum, and the parameters of the external fluid correspond to a cruise flight altitude of 25000 ft (i.e., 7628 m). Damping ratios for the structure and for the acoustic field of 1% were chosen to be representative of those in an aircraft [2, 26]. A large acoustic enclosure compared with the plates was chosen in order to simulate a more realistic approach of an aircraft cabin section. The flexible wall of the enclosure is composed by 50 simply supported identical plates (same dimensions and properties), with 5 panel rows along x-direction and 10 panel rows along y-direction. The panels have dimensions and properties similar to that of a typical commercial aircraft fuselage panel, representing the distance between adjacent frames and stringers. The fuselage cabin section is considered to start at x = 9.14 m from the nose of the aircraft, in order to consider a more realistic case of an aircraft fuselage section - as shown in [2], this is the start point of the forward section of a Boeing 727-200 airplane fuselage.

Table 1. Dimensions of the system.

Description	Symbol	Value, m
Plate length	a	0.5
Plate width	b	0.22
Plate thickness	h_p	0.00102
Enclosure length	L_x	2.5
Enclosure width	L_y	2.2
Enclosure height	L_z	2.1

Table 2. Properties of the physical system.

External Fluid:		
Description	Symbol	Value
Air density	ρ	0.54 Kg m^{-3}
Air kinematic viscosity	ν	2.85×10^{-5} m^2 s^{-1}
Speed of sound	c	309.6 m s^{-1}
Free stream velocity	U_∞	229.104 m s^{-1}
Convective velocity	U_c	0.7 U_∞
Empirical parameter	α_x	0.1
Empirical parameter	α_y	0.77
Panels:		
Description	Symbol	Value
Density	ρ_p	2800 Kg m^{-3}
Elasticity Modulus	E_p	7.24×10^{10} Pa^2
Poisson's ratio	ν	0.33
Damping ratio	ξ_p	0.01
Longitudinal tension	T_x	29300 N m^{-1}
Lateral tension	T_y	62100 N m^{-1}
Number of modes	M	
- unpressurized cabin: 44 (M_x=11, M_y=4)		
- pressurized cabin: 27 (M_x=9, M_y=3)		
Acoustic Enclosure:		
Description	Symbol	Value
Air density	ρ_0	1.2 Kg m^{-3}
Speed of sound	c_0	340 m s^{-1}
Damping ratio	ξ_{ac}	0.01
Number of modes	N	2912 (N_x=16, N_y=14, N_z=13)

5. RESULTS

5.1 Convergence

A convergence study was performed to determine the number of structural and acoustic modes required for the calculation of the spectral quantities. It was found that, for the frequency range of interest, [0; 1000] Hz, some non-resonant modes need to be considered.

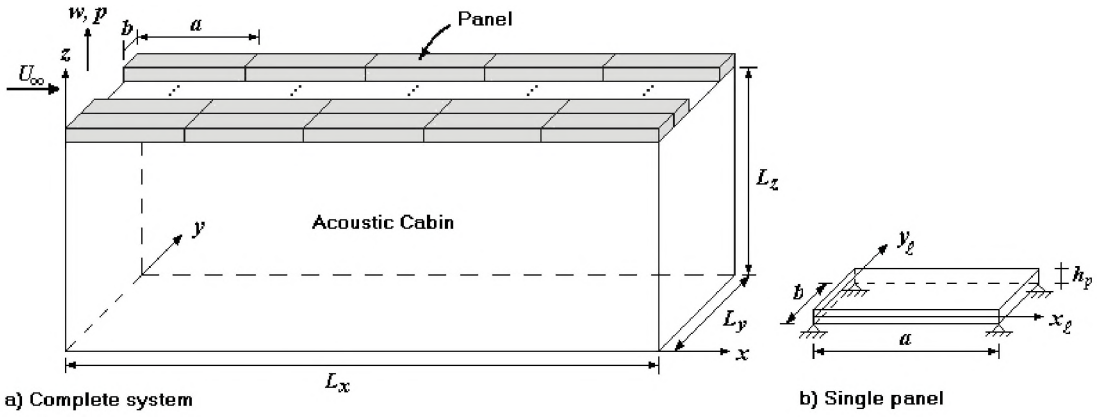

Figure 3. Geometry of the physical system.

A simple criterion to determine the number of structural modes required for convergence of the modal series up to a frequency f_{max} is the following: convergence is reached when the distance between two nodes of the structural mode shape is less than or equal to the half-wavelength of the bending wave on the plate, $\lambda_b/2$, at the analysis frequency, i.e.,

$$\frac{a}{M_x} \leq \frac{\lambda_b(\omega)}{2}, \tag{25}$$

$$\lambda_b(\omega) = 2\,\pi\,\omega^{-\frac{1}{2}} \left(\frac{D_p}{\rho_p h_p}\right). \tag{26}$$

Thus, for f_{max}=1000 Hz, from Eq.(25) one obtains $M_x \geq 11$. Another convergence criterion is presented in [16] - for a given upper frequency f_{max}, the number of modes (M_x,M_y) required for the calculation of the spectral quantities, for a tensioned panel, can be calculated by

$$\left\{\left[\left(\frac{M_x}{a}\right)^2 + \left(\frac{M_y}{b}\right)^2\right]^2 + \frac{T_x}{D_p}\left(\frac{M_x}{a}\right)^2 + \frac{T_y}{D_p}\left(\frac{M_y}{b}\right)^2\right\}^{1/4} \geq \left(\frac{\rho_p h_p}{D_p}\right)^{1/4} \sqrt{\frac{2\,f_{max}}{\pi}}. \tag{27}$$

For the untensioned plate case, the convergence criterion is obtained from Eq.(27) with in-plane tensions equal to zero. For the aircraft panel considered in the present study (for f_{max}=1000 Hz), the number of structural modes required to accurately calculate the PSD of the panel response is M_x=11 and M_y=4 for the untensioned plate, and M_x=9 and M_y=3 for the tensioned plate.

Table 3 displays the first 20 natural frequencies of the untensioned panel, and the corresponding frequencies for the in-tension panel. The number of enclosure acoustic modes required for the accurate calculation of the spectral quantities was also determined. Similarly to the plate, convergence is reached when the distance between two nodes of the acoustic mode shape is less or equal than half-wavelength of the acoustic wave in the interior of the enclosure, i.e.,

$$\frac{L_x}{N_x} \leq \frac{c_0}{2\,f_{max}}. \tag{28}$$

Thus, from Eq.(28) one obtains Nx ≥ 15. For the aircraft cabin considered and f_{max}=1000 Hz, the number of acoustic modes required to accurately calculate the PSD of the acoustic response is N_x=16, N_y=14 and N_y=13. The 2912 acoustic modes considered are plotted in Fig. 4, as well as the plate's mode lines for the untensioned and in-tension cases. As can be seen, several non-resonant modes need to be considered.

5.2 Hydrodynamic Coincidence

To study the effect of hydrodynamic coincidence, it is important to first identify the degree of matching between the boundary layer and the plate modes. Figure 5 shows the plate natural frequencies plotted against longitudinal mode number, m_x, for modes with m_y=1,...,4. Also plotted in this figure are the hydrodynamic coincidence lines (representing $f = m_x U_c/2a$) for three cases: $U_c = 0.7\,U_\infty$ (reference case), $U_c = 0.75\,U_\infty$ and $U_c = 0.8\,U_\infty$.

Table 3. Panels first 20 natural frequencies [Hz].

(m_x,m_y)	Untensioned panel	In-tension panel
(1,1)	61.44	355.45
(2,1)	91.34	402.11
(3,1)	141.17	473.89
(4,1)	210.93	566.52
(1,2)	215.87	711.41
(2,2)	245.77	742.08
(3,2)	295.60	793.07
(5,1)	300.62	677.62
(4,2)	365.36	864.22
(6,1)	410.25	806.19
(5,2)	455.05	955.41
(1,3)	473.26	1115.82
(2,3)	503.15	1142.37
(7,1)	539.81	952.05
(3,3)	552.98	1186.99
(6,2)	564.68	1066.51
(4,3)	622.75	1250.11
(8,1)	689.29	1115.36
(7,2)	694.24	1197.46
(5,3)	712.44	1332.24

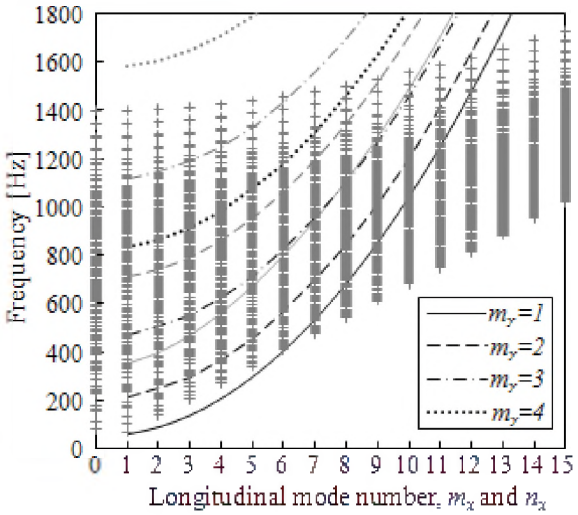

Figure 4. Matching between acoustic modes (+) and plates modes: untensioned (black lines), tensioned (grey lines).

From Fig. 5 one can confirm that hydrodynamic coincidence lines 'match' the plate modes over a large part of the frequency range, mainly for the untensioned plate case. As explained in [40], this confirms the importance of

inefficient, but resonant and highly excited modes in the aircraft noise problem. In the reference case, for the untensioned case, the plate modes (4,3), (12,3), (15,2) and (16,1) provide the best matching with the turbulent convecting scales ($m_x U_c/a\omega \approx 1$), and are thus highly excited modes. Of these 4 modes only (4,3) has a resonant frequency in the range of study, [0; 1000] Hz. For the tensioned case, the plate mode (3,1) provides the best matching with the hydrodynamic coincidence line. In the reference case, the hydrodynamic coincidence frequency, $f_c=\frac{U_c^2}{2\pi}\sqrt{\frac{\rho_p h_p}{D_p}}$, is 2580.74 Hz. Thus, in the frequency range under study all resonant and nonresonant modes considered are inefficient radiators.

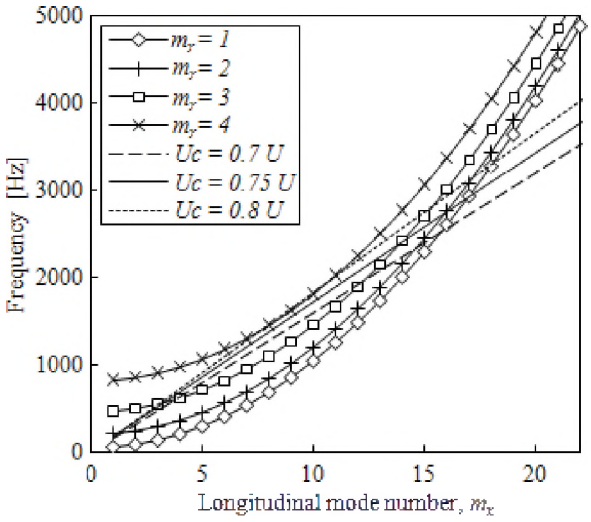

a) Untensioned Panel

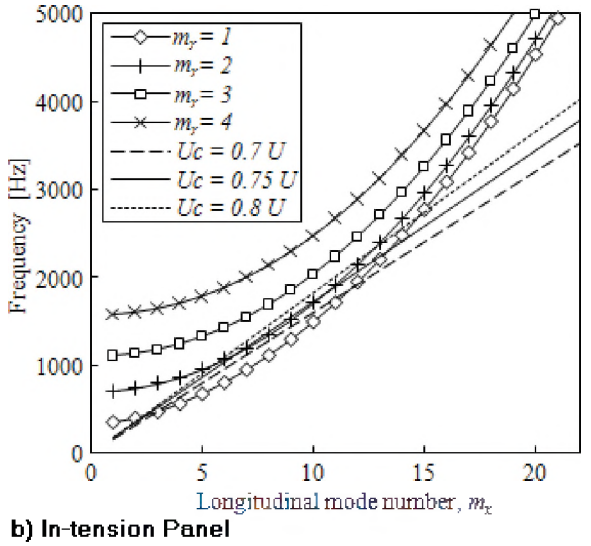

b) In-tension Panel

Figure 5. Matching between hydrodynamic coincidence lines and plate natural frequencies lines.

5.3 Frequency Resolution

All spectral quantities were obtained for the frequency range [0; 1000] Hz. The frequency resolution for the PSD calculations was obtained through an adaptive algorithm to meet the damping coefficient constraint, both for the untensioned and tensioned plates. This algorithm was developed to guarantee enough frequency resolution to resolve all resonance peaks within the frequency range covered (maximum frequency was determined based on the convergence study), for both structural and acoustic modes.

5.4 Predicted Structural Vibration Levels

The space-averaged plates displacement power spectral density (ADPSD), expressed by Eq.(23), and the plate displacement power spectral density (DPSD) in several points on the plates, given by Eq.(21), were obtained.

Figure 6 shows the ADPSD for the panel (1,1), i.e., panel located at first row of panels and first row of columns. Panels in other locations have similar ADPSD, with panels located at bigger x-coordinates having a slightly higher ADPSD at all frequencies. This can be explained since an increase in x-station results in a higher value for the reference PSD of the TBL excitation. The first 3 ADPSD peaks correspond to the bending modes (1,1), (3,1) and (5,1), for both untensioned and tensioned plates. Additionally, considering pressurization effects results in a decreased radiated ADPSD for lower frequencies compared with the unpressurized cabin. For the untensioned panel, a large response due to resonant amplification of (4,3) plate mode does not occur. This can be explained because, in the present case of study, hydrodynamic coincidence is not well tuned at frequencies where the hydrodynamic matching line broadly coincides with the resonant modes. For the tensioned plate, the mode (3,1), which provides the best matching with the hydrodynamic coincidence line, corresponds to the second ADPSD peak. This may be explained because (3,1) is the only plate mode which provides 'matching' with the hydrodynamic coincidence line, while for the untensioned plate a larger number of modes provide this matching.

The results for the DPSD are shown in Fig. 7, for three different locations in the surface of the plate (1,1), specifically at: (x_1, y_1)=(0.25,0.11)m, (x_2, y_2)=(0.1,0.06)m, and (x_3, y_3)=(0.4,0.06)m. DPSD plots for the other plates show similar results and, as for the ADPSD, it shows a slight overall increase with the increase of the x-coordinate. As shown in this figure, point 1, located at the center of the panel, follow the same line as the ADPSD, with the peaks located at the same frequencies. However, the same does not occur for the other points considered, in which additional peaks can be observed for the DPSD curves. This can be explained since the point at the center of the plate is not affected when the longitudinal mode number, m_x, or the lateral mode number, my, is even. Thus, when evaluating the PSD of the plate response, it is important to know the position of interest in the plate, since its value is dependent on the position of measurement. Comparing points 2 and 3 (both located at y = 0.06 m), one can conclude that points at higher x have generally bigger DPSD.

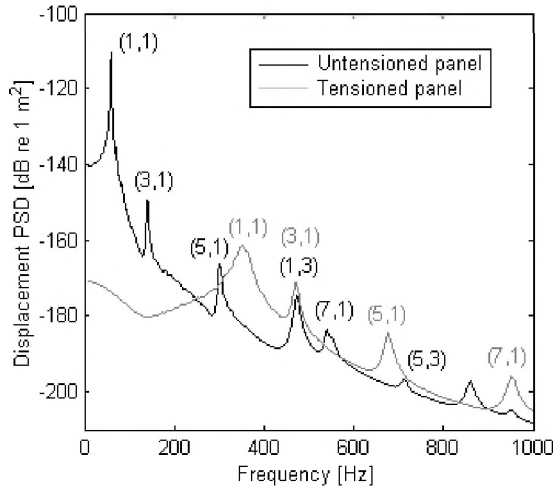

Figure 6. Space-averaged displacement PSD for plate (1,1).

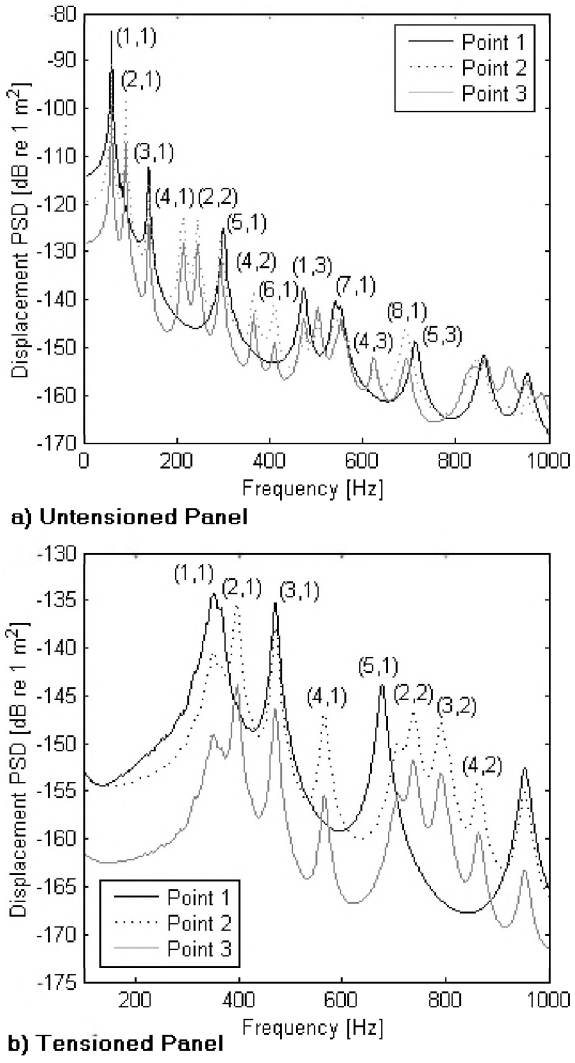

Figure 7. Displacement PSD at 3 points located at the surface of panel (1,1).

5.5 Predicted Cabin Sound Pressure Levels

The acoustic enclosure space-averaged pressure power spectral density (APPSD) and the acoustic pressure power spectral density (PPSD) at specific point in the enclosure, were obtained through Eqs.(24) and (22), respectively. The acoustic enclosure APPSD, due to the individual contribution of the panels, located at two different positions in the flexible wall, is shown in Fig. 8. An important conclusion to draw from this figure is that some peaks correspond to plate natural frequencies and other to acoustic natural frequencies. This illustrates the importance of the structural-acoustic coupling for accurate prediction of the internal pressure in the interior of an enclosure, such as for example an aircraft cabin. The uncoupled study of the sound radiated by an individual plate, vibrating due to turbulent flow, does not give the total information when the main goal is to predict aircraft interior noise. Another conclusion is that plates located at different positions have dissimilar contributions to the enclosure interior pressure levels. For instance, plate (3,7) has a negligible contribution in the amplification of the acoustic mode (1,0,0) compared with plate (1,1). Since plates in row 3 are located in the centre of the enclosure in the x-direction, they do not add significant contribution to the frequency associated to this mode, which has a node at centre of the enclosure in this direction. For the same reason, plates in row 3 have a decreased contribution for the amplification of all other modes with longitudinal mode number, n_x, equal to 1, compared with the other plates. All other modes (i.e., with longitudinal mode number equal to 0 or to 2) have similar mode amplification, since for modes with $n_x = 2$ the middle point correspond to an antinode, while for modes with $n_x = 0$ the pressure is constant along x-direction. For untensioned plates the interior SPL is bigger for lower frequencies, while for tensioned panels the maximum SPL is observed at higher frequencies. This occurs since the first plate mode increases from 61.44 Hz, in the unpressurized case, to 355.45 Hz in the pressurized case. However, for the pressurized case, frequencies below 355.45 Hz cannot be ignored, since several acoustic modes are amplified below this frequency.

Figure 9 shows the results for the interior pressure power spectral density (PPSD), at four chosen points inside the enclosure, due to the individual radiation of plates, located at four different positions - specifically, plates (1,1), (3,1), (3,5), and (5,1) are analyzed. The points inside the enclosure under study are the following (defined in the global coordinates system): $(x_1, y_1, z_1)=(x_{pi}+a/2, y_{pi}+b/2, 2)$ and $(x_2, y_2, z_2)=(x_{pi}+a/2, y_{pi}+b/2, 1)$, $(x_3, y_3, z_3)=(1,1,2)$, and $(x_4, y_4, z_4)=(1,1,1)$. Note that points 1 and 2 are different for each plate, with x_{pi} and y_{pi} corresponding to the initial x and y coordinates of each plate. It can be observed that point (x_1, y_1, z_1) has higher PPSD at almost all frequencies, compared with the other points. As expected, decreasing z-coordinate (i.e., moving away from the plates) results in lower PPSD values. It is interesting to verify that the structural-acoustic

coupling has an important role in the prediction of the interior SPL.

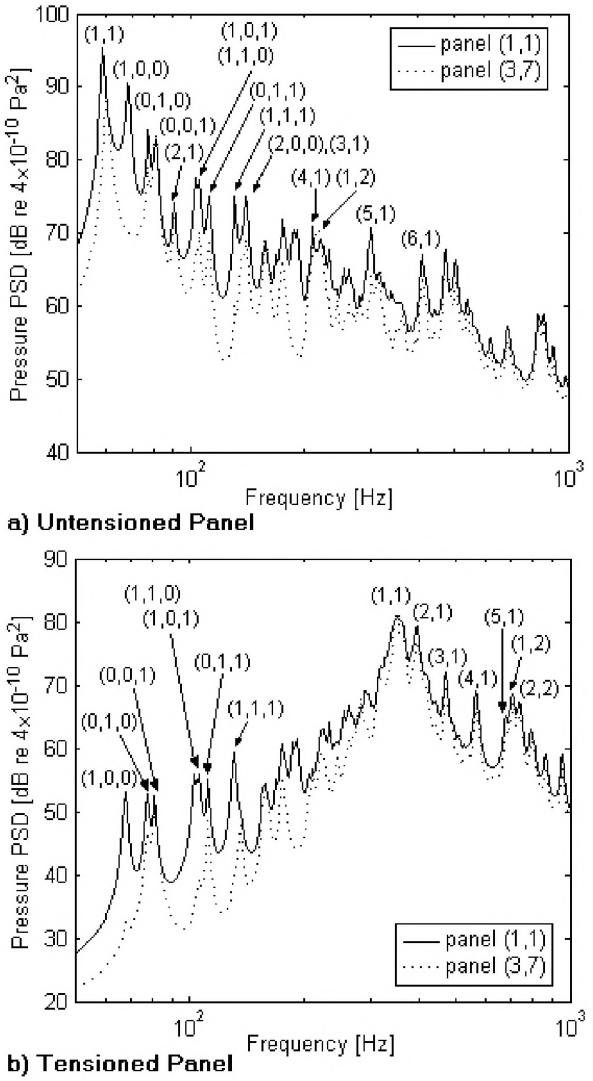

Figure 8. Space-averaged pressure PSD, for the contribution of panels (1,1) and (3,7).

Analyzing the results for the four different plates, and the same observing point (x_1, y_1, z_1), one can verify that the PPSD plot has some variations from plate to plate. Since point (x_1, y_1, z_1) is always at the same relative position at each plate, that difference can only be due to the enclosure acoustic modes. If only the plate modes were considered, one would obtain the similar curves for all plates in point (x_1, y_1, z_1), and as well in point (x_2, y_2, z_2), which is not what is observed. The fact that each plate is in a different position with relation to the enclosure global coordinate system, changes the way it couples with the acoustic enclosure. This explains why plates (1,1) and (5,1) have similar curves for points (x_1, y_1, z_1) and (x_2, y_2, z_2). As concluded for the DPSD, when evaluating the PSD of the interior pressure is important to know which is the position of interest in the enclosure, since the SPL value is dependent on the position of measurement.

6. CONCLUSIONS

An analytical study to predict the turbulent boundary layer-induced noise in the interior of a rectangular enclosure with one flexible wall, consisting of several panels, is presented. Predictions of the space-averaged PSD and localized PSD were obtained for the displacement of the plates and interior acoustic pressure in the enclosure. The characteristics of the physical system were selected to represent an aircraft cabin, and the external flow considered is representative of typical cruise conditions of a commercial aircraft. The analytical model is based on modal analysis, and it considers the structural-acoustic coupling for frequencies up to 1000 Hz. A convergence study was performed to determine the number of structural and acoustic modes required for the calculation of the spectral quantities, indicating that a large number of non-resonant modes need to be considered in the analysis. Also, it was found that hydrodynamic coincidence lines 'match' the plate modes over a large part of the frequency range, confirming the importance of inefficient, but resonant and highly excited modes in the aircraft noise problem.

This study leads to conclude that, for the accurate prediction of aircraft interior noise, the position of the panel as well as the structural-acoustic coupling effects are important factors to consider. Thus, the traditional approach of assuming a single panel vibrating to free air or coupled with an acoustic enclosure needs to consider these two factors. Additionally, the space-averaged PSD values only give information about the mean value. If one desires to determine the localized PSD values (for the plate vibration or for the interior pressure level), then the space-averaged values may not sufficiently accurate, since predicted averaged and localized values are dissimilar. For instance, one might want to predict the interior SPL at the passenger's head height, while in flight.

The analytical model presents also a solid basis for further analyzes, such as multidisciplinary design optimization analysis, and design and implementation of noise reduction techniques, as for instance: the use of added masses in the structure as passive noise control methods; the use of structural actuators embedded in the plates as active structural acoustic control methods; or loudspeakers installed at the interior of the cabin as active control noise methods.

ACKNOWLEDGMENTS

The authors are grateful for the financial support of the Foundation for Science and Technology, through a post-graduate scholarship program.

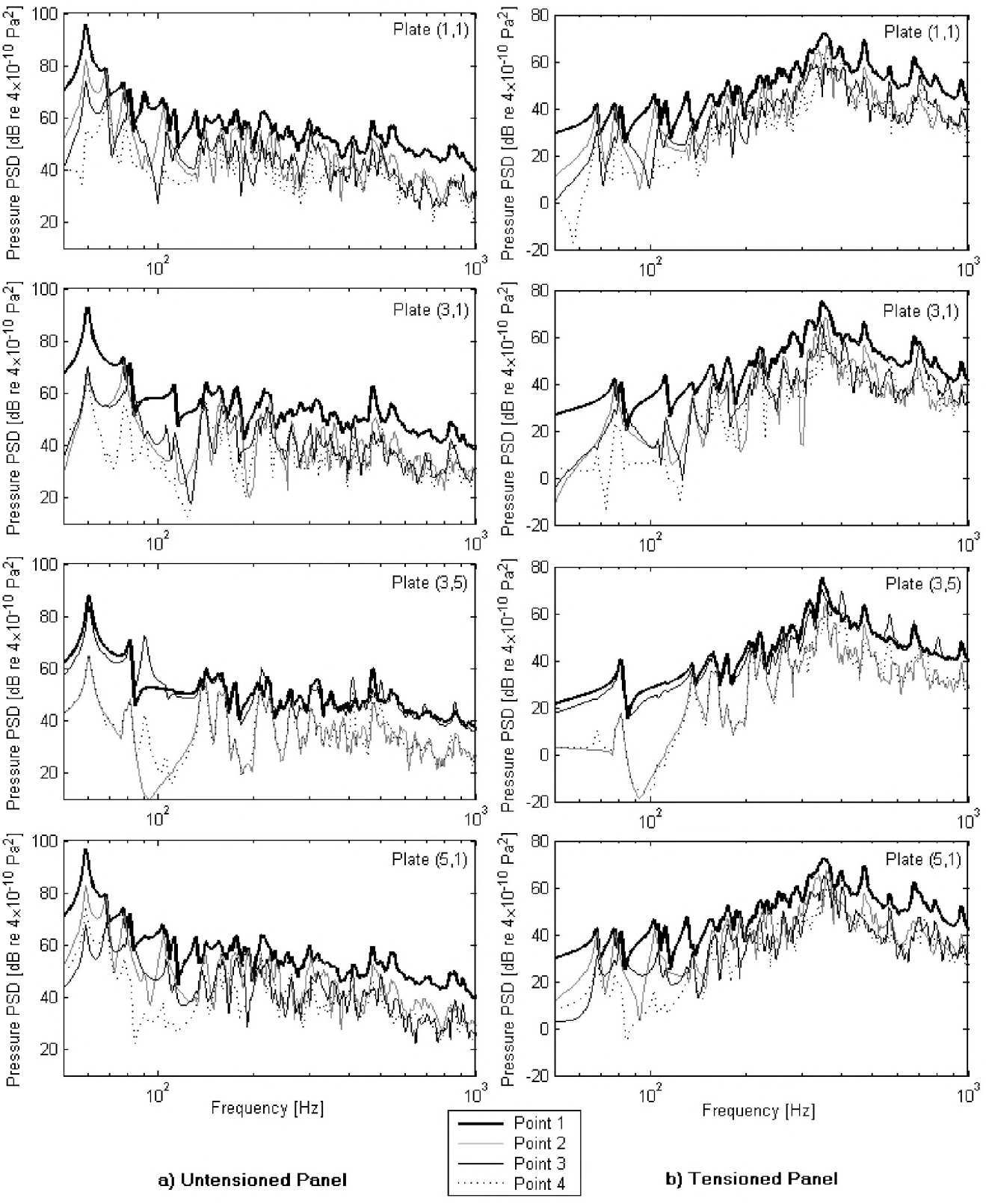

Figure 9. Pressure PSD at 4 points inside the enclosure, for the individual contribution of panels (1,1), (3,1), (3,5), and (5,1).

REFERENCES

[1] D. E. Bishop, Cruise flight noise levels in a turbojet transport airplane. *Noise Control* (1961), 7, pp. 37-42.

[2] W. V. Bhat, Flight test measurement of measurement of exterior turbulent boundary layer pressure fluctuations on Boeing Model 737 airplane. *Journal of Sound and Vibration* (1971), 14 (4), pp. 439-457.

[3] W. V. Bhat and J. F. Wilby, Interior noise radiated by an airplane fuselage subjected to turbulent boundary layer excitation and evaluation of noise reduction treatments. *Journal of Sound and Vibration* (1971), 18 (4), pp. 449-464.

[4] G. P. Gibbs, R. H. Cabell and J. Juang, Controller Complexity for Active Control of Turbulent Boundary-Layer Noise from Panels. *AIAA Journal* (2004), 42(7), pp. 1314-1320.

[5] R. E. Hayden, B. S. Murray, and M. A. Theobald, A Study of Interior Noise Levels, Noise Sources and Transmission Paths in Light Aircraft, *NASA CR-172152* (1983).

[6] S. P. Engelstad, Computational modeling considerations for aircraft cockpit noise, *15th AIAA Aeroacoustic Conference*, Long Beach, CA, (1993), pp. 25–37.

[7] K. D. Frampton and R. L. Clark, Power flow in an aeroelastic plate backed by a reverberant cavity. *Journal of the Acoustical Society of America* (1997), 102(3), pp. 1620-1627.

[8] J. da Rocha, A. Suleman and F. Lau. Prediction of flow-induced noise in transport vehicles: development and validation of a coupled structural-acoustic analytical framework, *Canadian Acoustics* (2009), 37(4), pp. 13-29.

[9] D. A. Bies, A review of flight and wind tunnel measurements of boundary layer pressure fluctuations and induced structural response, *NASA CR-626* (1966).

[10] L. Maestrello, Measurement of noise radiated by turbulent boundary layer excited panels. *Journal of Sound and Vibration* (1965), 2(2), pp. 100-115.

[11] J. F. Wilby and F. L. Gloyna, Vibration measurements of an airplane fuselage structure I. Turbulent boundary layer excitation. *Journal of Sound and Vibration* (1972), 23(4), pp. 443-466.

[12] J. F. Wilby, Aircraft interior noise. *Journal of Sound and Vibration* (1996), 190 (3), pp. 545-564.

[13] W. A. Strawderman, Turbulent-flow-excited vibration of a simply supported, rectangular flat plate. *The Journal of the Acoustical Society of America* (1969), 45(1), pp. 177-192.

[14] H. G. Davies, Sound from turbulent boundary-layer-excited panels. *The Journal of the Acoustical Society of America* (1971), 49(3), pp. 879-889.

[15] R. L. Clark and K. Frampton, Aeroelastic structural acoustic coupling: implications on the control of turbulent boundary-layer noise transmission. *Journal of the Acoustical Society of America* (1997), 102(3), pp. 1639-1647.

[16] C. Maury, P. Gardonio and S.J. Elliot, A wavenumber approach to the modeling the response of a random excited panel, Part II: application to aircraft panels excited by a turbulent boundary layer. *Journal of Sound and Vibration* (2002), 252(1), pp. 115-139.

[17] J. Park, T. Siegmund and L. Mongeau, Analysis of the flow-induced vibration of viscoelastically supported rectangular plates. *Journal of Sound and Vibration* (2003), 261(2), pp. 225-245.

[18] C. K. Barton and E. F. Daniels, Noise transmission through flat rectangular panels into a closed cavity, *NASA TP-1321* (1978).

[19] R. Vaicaitis and M. Slazak, Noise transmission through stiffened panels. *Journal of Sound and Vibration* (1980), 70(3), pp. 413-426.

[20] G. Corcos, Resolution of pressure in turbulence. *Journal of the Acoustical Society of America* (1963), 35(2), pp. 192-199.

[21] G. Corcos, The structure of the turbulent pressure field in boundary layer flows. *Journal of Fluid Mechanics - Cambridge Journal Online* (1964), 18, pp. 353-378.

[22] B. M. Efimtsov, Characteristics of the field of turbulent wall pressure fluctuations at large Reynolds numbers. *Soviet Physics-Acoustics* (1982), 28 (4), pp. 289-292.

[23] D. M. Chase, The character of the turbulent wall pressure spectrum at subconvective wavenumbers and a suggested comprehensive model. *Journal of Sound and Vibration* (1987), 112, pp. 125-147.

[24] J. E. Ffowcs Williams, Boundary-layer pressures and the Corcos model: a development to incorporate low wavenumber constraints. *Journal of Fluid Mechanics* (1982), 125, pp. 9-25.

[25] A. V. Smol'yakov and V. M. Tkachenko, Model of a field of pseudonic turbulent wall pressures and experimental data. *Soviet Physics-Acoustics* (1991), 37 (6), pp. 627-631.

[26] C. Maury, P. Gardonio and S. J. Elliot, Active control of the flow-induced noise transmitted through a panel. *AIAA Journal* (2001), 39(10), pp. 1860-1867.

[27] F. Han, L. G. Mongeau and R. J. Bernhard, A model for the vibro-acoustic response of plates excited by complex flows. *Journal of Sound and Vibration* (2001), 246(5), pp. 901-926.

[28] C. Maury, P. Gardonio and S. J. Elliot, Model for the active control of flow-induced noise transmitted through double partitions. *AIAA Journal* (2002), 40(6), pp. 1113-1121.

[29] S. J. Elliot, C. Maury and P. Gardonio, The synthesis of spatially correlated random pressure fields. *Journal of the Acoustical Society of America* (2005), 117(3), pp. 1186-1201.

[30] J. Rohlfing and P. Gardonio, Active Control of Sound Transmission through Panels with Flexible Boundaries under Deterministic and Stochastic Excitation, *Institute of Sound and Vibration Research (ISVR) Technical Memorandum 977* (2007).

[31] W. R. Graham, A comparison of models for the wavenumber frequency spectrum of turbulent boundary layer pressures. *Journal of Sound and Vibration* (1997), 206(4), pp. 541-565.

[32] R. Rackl and A. Weston, Modeling of turbulent boundary layer surface pressure fluctuation auto and cross spectra - verification and adjustments based on TU-144LL data, *NASA CR-213938* (2005).

[33] J. F. Wilby and F. L. Gloyna, Vibration measurements of an airplane fuselage structure II. Jet noise excitation. *Journal of Sound and Vibration* (1972), 23 (4), pp. 467-486.

[34] A. C. Jackson et al, Transport composite fuselage technology - impact dynamics and acoustic transmission, *NASA CR-4035* (1986).

[35] D. Palumbo, R. Cabell, J. Cline, and B. Sullivan, Active structural interior noise on acoustic noise of Raytheon 1900D, *NASA TM-209846* (2000).

[36] S. A. Rizzi, R. G. Rackl, J. Cline and E. V. Andrianov, Flight test measurements from the Tu-144LL structure/cabin noise experiment, *NASA TM-209858* (2000).

[37] T. H. Beier, W. V. Bhat, S. A. Rizzi, R. J. Silcox and M. A. Simpson, High speed research program structural acoustics multi-year summary report, *NASA TM-213536* (2005).

[38] C. Maury, P. Gardonio and S. J. Elliot, A wavenumber approach to modeling the response of a randomly excited panel, part I: general theory. *Journal of Sound and Vibration* (2002), 252(1), pp. 83-113.

[39] R. Wahidi, W. Chakroun and S. Al-Fahed, The behavior of the skin friction coefficient of a turbulent boundary layer flow over a flat plate with differently configured transverse square grooves, *Experimental Thermal and Fluid Science* (2005), 30(2), pp. 141–152.

[40] W. R. Graham, Boundary layer induced noise in aircraft, Part I: the flat plate model, *Journal of Sound and Vibration* (1996), 192(1), pp. 101–120.